THE JOURNAL OF PHYSICAL CHEMISTRY Letters

Letter

pubs.acs.org/JPCL

Two-Dimensional Transition Metal Dichalcogenide Alloys: Stability and Electronic Properties

Hannu-Pekka Komsa*,† and Arkady V. Krasheninnikov†,‡

†Department of Physics, University of Helsinki, P.O. Box 43, 00014 Helsinki, Finland

‡Department of Applied Physics, Aalto University, P.O. Box 11100, 00076 Aalto, Finland

ABSTRACT: Using density-functional theory calculations, we study the stability and electronic properties of single layers of mixed transition metal dichalcogenides (TMDs), such as $MoS_{2x}Se_{2(1-x)}$, which can be referred to as two-dimensional (2D) random alloys. We demonstrate that mixed $MoS_2/MoSe_2/MoTe_2$ compounds are thermodynamically stable at room temperature, so that such materials can be manufactured using chemical-vapor deposition technique or exfoliated from the bulk mixed materials. By applying the effective band structure approach, we further study the electronic structure of the mixed 2D compounds and show that general features of the band structures are similar to those of their binary constituents. The direct gap in these materials can continuously be tuned, pointing toward possible applications of 2D TMD alloys in photonics.

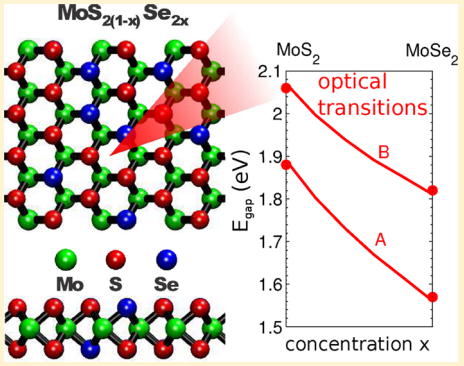

SECTION: Plasmonics, Optical Materials, and Hard Matter

In many bulk ternary semiconductor compounds, such as GaInAs[1] or CdZnTe,[2] the band gap depends continuously on constituent composition, making it possible to tune the electronic and optical properties of these materials for uses in specific applications, such as solar cells, radiation detectors, or gas sensors.[3,4] These compounds are random substitutional alloys without translational long-range order.

Recently, several two-dimensional (2D) materials, such as graphene,[5] hexagonal boron-nitride (h-BN),[6] and silica bilayer[7,8] were manufactured. These nanostructures possess many fascinating properties that can be used in various applications.[9] Notably, graphene is a semimetal, while h-BN is a wide gap semiconductor. Taking into account the similarities in the atomic structure of these two materials, the possibilities for creating a mixed BCN system with a gap tunable by component concentration have been envisioned. However, theory[10,11] and experiments[12] have indicated that 2D BCN materials are thermodynamically unstable and that h-BN and graphene tend to segregate.

This approach, however, may prove to be successful in 2D transition metal dichalcogenides (TMDs). Most of the bulk TMDs are layered compounds with a common structural formula $MeCh_2$, where Me stands for transition metals (Mo, W, Ti, etc.) and Ch for chalcogens (S, Se, Te), similar crystal structure and lattice constants. Like graphene and h-BN, 2D TMDs can be manufactured not only by mechanical[9,13] and chemical[14,15] exfoliation of their layered bulk counterparts, but also directly by chemical vapor deposition (CVD)[16−18] or two-step thermolysis.[19] These 2D materials are expected to have electronic properties varying from metals to wide-gap semiconductors, as their bulk counterparts,[20,21] and excellent mechanical characteristics.[22,23] Several nanoelectronic[13,24] and photonic[25,26] applications have already been demonstrated using these 2D materials.

The large variety of different atomic species among the TMD class of materials holds promise for engineering of nanoscale devices. Moreover, as mixing has been previously realized in the bulk, both in the metal (e.g., $Mo_xW_{1-x}S_2$[27−29]) and chalcogen sublattices (e.g., $MoS_{2x}Se_{2(1-x)}$[30−33]), 2D mixed compounds may also be stable and possess intriguing electronic properties. However, the thermodynamic stability, which is of particular importance for CVD-related growth methods, and electronic properties of 2D mixed TMDs have not yet been studied.

In this Letter, using first-principles calculations, we study the stability, that is, the mixing/segregation behavior, of 2D TMD alloys. We evaluate the free energy of mixing for $MoS_2/MoSe_2/MoTe_2$ systems. We also discuss which local atomic configurations are energetically favorable. We further employ the concept of effective band structure (EBS), recently suggested by Popescu and Zunger,[34] and study the electronic and optical properties of the mixed materials.

In all calculations in this work, we employed the density-functional theory (DFT) with the exchange-correlation functional of Perdew, Burke and Ernzerhof (PBE)[35] and the projector augmented wave formalism as implemented in the simulation package VASP.[36,37] We use plane wave cutoff of 500 eV and **k**-point sampling corresponding to 10 × 10 × 1 of the primitive cell Brillouin zone, which were found to produce total energies converged within 1 meV.

Received: October 17, 2012
Accepted: November 22, 2012

   dx.doi.org/10.1021/jz301673x | J. Phys. Chem. Lett. 2012, 3, 3652−3656

A cartoon illustrating the atomic structure of a mixed 2D TMD, along with the constituent parent materials is shown in Figure 1. In practice, the alloys are modeled by 5 × 5 supercells.

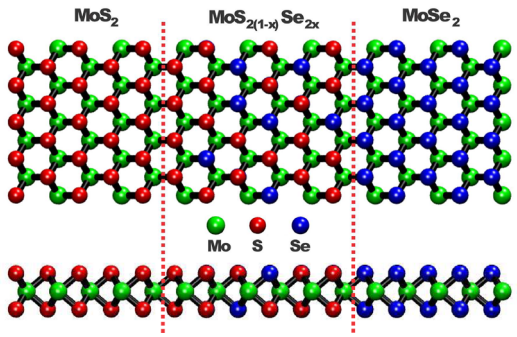

Figure 1. Top and side views of the atomic structures of MoS_2 (left), $MoS_{2x}Se_{2(1-x)}$ alloy (middle), and $MoSe_2$ (right) 2D TMDs. Note that the systems consist of three layers of atoms.

To collect statistics, up to ten supercells with randomly placed atoms are constructed for every alloy composition. The lattice constants are taken from a linear interpolation between the constituents. The Vegard's law has been experimentally found to hold well for the a lattice constant[30,33] of bulk TMD alloys, as also verified by our test calculations for several 2D systems. We define the free energy of mixing as

$$F_{\mathrm{mix}}(x) = E_{\mathrm{mix}}(x) - TS_{\mathrm{mix}}(x) \quad (1)$$

where $E_{\mathrm{mix}}(x)$ is the internal energy of mixing:

$$E_{\mathrm{mix}}(x) = E_{\mathrm{A}_x\mathrm{B}_{1-x}} - [xE_{\mathrm{A}} + (1-x)E_{\mathrm{B}}] \quad (2)$$

A and B are the constituent binary compounds, such as A = MoS_2 and B = $MoSe_2$, and $0 < x < 1$, as usual. Mixing entropy per cell is evaluated through[38]

$$S_{\mathrm{mix}}(x) = -2[x \ln x + (1-x)\ln(1-x)]k_{\mathrm{B}} \quad (3)$$

We assumed here that the vibrational modes are similar in all cases, and the corresponding contributions cancel out.

In Figure 2 we show the mixing energies of the MoS_2/$MoSe_2$/$MoTe_2$ system. As Mo sublattice is the same in both materials, in what follows, x is the relative concentration of chalcogen atoms. The internal energy of mixing for $MoTe_2$/MoS_2 and $MoSe_2$/$MoTe_2$ alloys is positive, although small. Interestingly, it is negative for nearly all configurations of

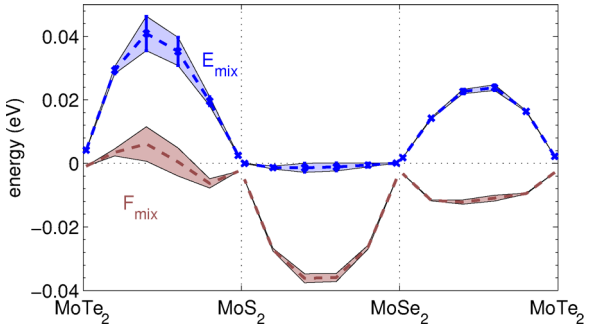

Figure 2. Internal E_{mix} and free F_{mix} energies of mixing per primitive cell for the MoS_2/$MoSe_2$/$MoTe_2$ 2D alloys. The width of the shaded areas denotes one standard deviation of the variation in calculated energies.

MoS_2/$MoSe_2$ alloy, and the mixture should be energetically favored over the segregated phases even at 0 K. This behavior is enabled by the 2D structure of the system: all chalcogen atoms are at the surface, and the structure is free to relax. The entropic contributions promote the mixing even further and should lead to mixing of all considered alloys under thermodynamic equilibrium at temperatures above 300 K. Due to the weak van der Waals interactions between the layers, we expect the mixing energies to be similar also for the bulk systems. Thus, such 2D alloys should be attainable either through exfoliation[9,14,15] from the bulk phase,[32,39] or by monolayer growth using CVD techniques[16−18] or thermolysis.[19] In addition, alloying could be achieved through vacancy production and atomic substitution under electron beam.[40]

In order to analyze the electronic structure of 2D random alloys, we employed the EBS approach.[34] Formally, random substitutional alloys lack translational symmetry, and thus the conventional band picture is broken. Yet, the experimental data from alloys is often interpreted in terms of quantities, such as effective masses and van Hove singularities, that are derived from the band dispersion. This difficulty may be overcome by constructing large supercells with randomly distributed atoms, and transforming the eigenstates into an EBS in the primitive cell using a spectral decomposition. This shows how various band structure characteristics are preserved or transformed during the mixing.

A representative band structure for $MoS_{2(0.6)}Se_{2(1-0.6)}$ alloy is shown in Figure 3 together with those of the corresponding

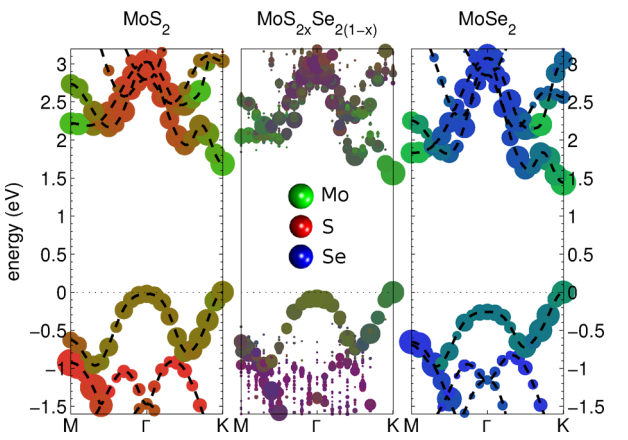

Figure 3. The effective band structures of MoS_2, $MoS_{2(0.6)}Se_{2(1-0.6)}$ alloy, and $MoSe_2$. The size of the sphere denotes the magnitude of the projection to the corresponding primitive cell **k**-point. The color denotes the Mo/S/Se weight of the states. For MoS_2 and $MoSe_2$, the band structures obtained from primitive cell calculation are overlaid with dashed lines.

constituents. The size of the sphere denotes the magnitude of the projection, and the color denotes the weight of each atomic species. The band structure is generally very similar to those of its constituents, MoS_2 and $MoSe_2$, with only very minor mixing throughout the Brillouin zone. There are no strong S or Se localized states in the alloy EBS, meaning that the wave functions are delocalized and "bulk-like". The band gap thus appears to be well-defined, with the conduction band minimum (CBM) and valence band maximum (VBM) located at the K-point. The gap is direct, and due to the Mo-character of the band edges at the K-point, the effect of chalcogen mixing on these states is small.

dx.doi.org/10.1021/jz301673x | J. Phys. Chem. Lett. 2012, 3, 3652−3656

In Figure 4 we present the calculated band gaps together with the estimated optical gaps. For the latter, the calculated band gaps are corrected to match the measured optical transitions of the binary constituents.[41] In the case of alloys, the corrections are linearly interpolated, thereby retaining the calculated band gap bowing (deviation from linear behavior). The results demonstrate that the band gap can be continuously changed depending on the composition, indicating that the mixing approach can be beneficial for optoelectronic applications. Band gaps of the $MoS_{2x}Se_{2(1-x)}$ alloys are mostly in the red part of the visible spectrum (1.65−2.0 eV), whereas the gaps for Te-containing alloys move well into the infrared region.

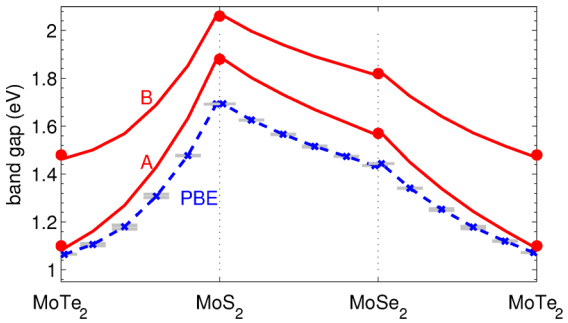

Figure 4. Band gaps of $MoS_2/MoSe_2/MoTe_2$ alloys as functions of relative concentrations of their constituents. The dashed (blue) line denotes the calculated gaps, whereas the two solid (red) lines correspond to the experimentally resolved A and B optical transitions. The experimental values at the binary limits are taken from ref 41 and the bowing from calculations.

All the above results were calculated with same chalcogen concentration at the upper and lower chalcogen layers. During the growth of these alloys, such balance is likely to be broken, at least locally. Therefore, we studied how the mixing energies depend on the concentration imbalance, by allowing the concentrations in the two layers (x_{down} and x_{up}) to change, within the constraint $x = (x_{down} + x_{up})/2$. As shown in Figure 5a for $MoS_{2(0.6)}Se_{2(1-0.6)}$, such imbalance is energetically unfavorable. If it still occurs during the growth, the mixing energy (at 0 K) becomes positive, but only slightly. The entropic contributions are still considerably larger and will make the mixing favored, even at room temperature.

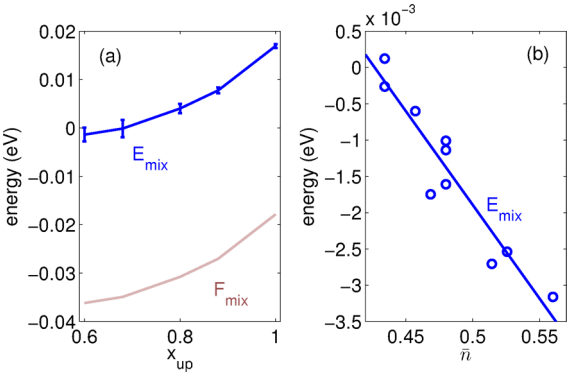

Figure 5. (a) Mixing energy of the $MoS_{2(0.6)}Se_{2(1-0.6)}$ alloy as a function of the S concentration on the upper chalcogen layer x_{up}. Consequently, on the lower layer, $x_{down} = 2{\cdot}0.6 - x_{up}$. (b) The mixing energy of 10 configurations of $MoS_{2(0.6)}Se_{2(1-0.6)}$ with respect to the number of S−Se nearest neighbor bonds.

We also studied in more detail the favored short-range ordering of these alloys. In order to quantify the mixing, we calculate the fraction of dissimilar chalcogen pairs (e.g., S−Se) in the nearest neighbor chalcogen sites (six sites, cf. Figure 1) averaged over all sites $\bar{n} = \langle n^{NN}_{S-Se}/6 \rangle$. In Figure 5b we plot the mixing energy for each supercell as a function of $\bar{n}$. The correlation indicates that the lowest energy configurations are the ones that maximize the number of dissimilar atom pairs (S−Se) in the nearest atomic sites and correspondingly minimize the number of nearest neighbors of the same type (S−S and Se−Se). For the $MoS_{2x}Se_{2(1-x)}$ system, the variation in formation energies is still extremely small (few meV), and there is no preference for any particular configuration. However, the tendency is stronger in the Te-containing alloys, as also indicated by the larger deviation of formation energies in Figure 2.

Finally, we addressed the possibilities of engineering the band structure of 2D TMDs by mixing the atoms in the metal sublattice. As a typical structure, we considered the $Mo_xW_{1-x}S_2$ alloy. As evident from Figure 6, the mixing energy is negative, of similar magnitude to S/Se results. The variation in the mixing energies is found to be very small without any tendency for short-range ordering, which can be assigned to the chemical "similarity" of the Mo and W. The calculated PBE band gaps also vary by only 0.14 eV, but extend the range of band gaps obtainable from these alloys. In addition, the large difference in the spin−orbit splitting of the VBM at the K-point, and consequently in the separation of the A and B transitions, could prove useful in spin- and valleytronic applications.[43−45]

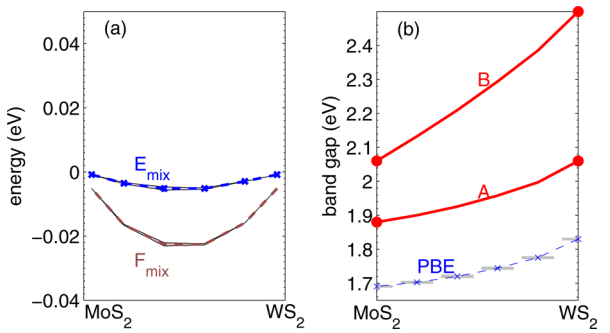

Figure 6. (a) Internal E_{mix} and free F_{mix} energies of mixing per primitive cell for the MoS_2/WS_2 alloy. (b) Band gaps of the alloy. The experimental data for the constituents are taken from refs 41 and 42 and the bowing obtained from calculations.

In conclusion, using DFT calculations, we demonstrated that mixing energy of Mo containing TMD alloys is low and that mixed ternary $MoS_2/MoSe_2/MoTe_2$ 2D compounds are thermodynamically stable at room temperature. This indicates that such materials can be manufactured using chemical-vapor deposition technique or exfoliated from the bulk mixed counterparts. The short-range atomic order favors having dissimilar atoms in the nearest neighbor sites in the chalcogen sublattice. Most importantly, the band gap is direct and may be continuously tuned between the constituent limits, indicating that the mixing approach can be beneficial for optoelectronic applications.

dx.doi.org/10.1021/jz301673x | J. Phys. Chem. Lett. 2012, 3, 3652−3656

AUTHOR INFORMATION

Corresponding Author

*E-mail: hannu-pekka.komsa@helsinki.fi.

Notes

The authors declare no competing financial interest.

ACKNOWLEDGMENTS

We acknowledge financial support by the Academy of Finland through projects 218545 and 263416, and the University of Helsinki Funds. We also thank CSC Finland for generous grants of computer time.

REFERENCES

(1) Vurgaftman, I.; Meyer, J. R.; Ram-Mohan, L. R. Band Parameters for III−V Compound Semiconductors and Their Alloys. *J. Appl. Phys.* **2001**, *89*, 5815.

(2) Del Sordo, S.; Abbene, L.; Caroli, E.; Mancini, A. M.; Zappettini, A.; Ubertini, P. Progress in the Development of CdTe and CdZnTe Semiconductor Radiation Detectors for Astrophysical and Medical Applications. *Sensors* **2009**, *9*, 3491−3526.

(3) Pfeiler, W., Ed. *Alloy Physics: A Comprehensive Reference*; Wiley-VCH: Weinheim, Germany, 2007.

(4) Chen, A.-B., Sher, A., Eds. *Semiconductor Alloys: Physics and Materials Engineering*; Plenum Press: New York, 1995.

(5) Geim, A. K.; Novoselov, K. S. The Rise of Graphene. *Nat. Mater.* **2007**, *6*, 183−191.

(6) Pacilé, D.; Meyer, J. C.; Girit, Ç. Ö.; Zettl, A. The Two-Dimensional Phase of Boron Nitride: Few-Atomic-Layer Sheets and Suspended Membranes. *Appl. Phys. Lett.* **2008**, *92*, 133107.

(7) Lichtenstein, L.; Büchner, C.; Yang, B.; Shaikhutdinov, S.; Heyde, M.; Sierka, M.; Włodarczyk, R.; Sauer, J.; Freund, H.-J. The Atomic Structure of a Metal-Supported Vitreous Thin Silica Film. *Angew. Chem., Int. Ed.* **2012**, *51*, 404−407.

(8) Huang, P. Y.; Kurasch, S.; Srivastava, A.; Skakalova, V.; Kotakoski, J.; Krasheninnikov, A. V.; Hovden, R.; Mao, Q.; Meyer, J. C.; Smet, J.; Muller, D. A.; Kaiser, U. Direct Imaging of a Two-Dimensional Silica Glass on Graphene. *Nano Lett.* **2012**, *12*, 1081−1086.

(9) Novoselov, K. S.; Jiang, D.; Schedin, F.; Booth, T. J.; Khotkevich, V. V.; Morozov, S. V.; Geim, A. K. Two-Dimensional Atomic Crystals. *Proc. Natl. Acad. Sci. U.S.A.* **2005**, *102*, 10451−10453.

(10) da Rocha Martins, J.; Chacham, H. Disorder and Segregation in B−C−N Graphene-Type Layers and Nanotubes: Tuning the Band Gap. *ACS Nano* **2011**, *5*, 385−93.

(11) Yuge, K. Phase Stability of Boron Carbon Nitride in a Heterographene Structure: A First-Principles Study. *Phys. Rev. B* **2009**, *79*, 144109.

(12) Ci, L.; Song, L.; Jin, C. H.; Jariwala, D.; Wu, D. X.; Li, Y. J.; Srivastava, A.; Wang, Z. F.; Storr, K.; Balicas, L.; Liu, F.; Ajayan, P. M. Atomic Layers of Hybridized Boron Nitride and Graphene Domains. *Nat. Mater.* **2010**, *9*, 430−435.

(13) Radisavljevic, B.; Radenovic, A.; Brivio, J.; Giacometti, V.; Kis, A. Single-Layer MoS_2 Transistors. *Nat. Nanotechnol.* **2011**, *6*, 147−150.

(14) Eda, G.; Yamaguchi, H.; Voiry, D.; Fujita, T.; Chen, M.; Chhowalla, M. Photoluminescence from Chemically Exfoliated MoS_2. *Nano Lett.* **2011**, *11*, 5111−5116.

(15) Coleman, J. N.; Lotya, M.; O'Neill, A.; Bergin, S. D.; King, P. J.; Khan, Umar; Young, K.; Gaucher, A.; De, S.; Smith, R.; et al. Two-Dimensional Nanosheets Produced by Liquid Exfoliation of Layered Materials. *Science* **2011**, *331*, 568−571.

(16) Kim, D.; Sun, D.; Lu, W.; Cheng, Z.; Zhu, Y.; Le, D.; Rahman, T. S.; Bartels, L. Toward the Growth of an Aligned Single-Layer MoS_2 Film. *Langmuir* **2011**, *27*, 11650−11653.

(17) Zhan, Y.; Liu, Z.; Najmaei, S.; Ajayan, P. M.; Lou, J. Large-Area Vapor-Phase Growth and Characterization of MoS_2 Atomic Layers on a SiO_2 Substrate. *Small* **2012**, *8*, 966−971.

(18) Lee, Y.-H.; Zhang, X.-Q.; Zhang, W.; Chang, M.-T.; Lin, C.-T.; Chang, K.-D.; Yu, Y.-C.; Wang, J. T.-W.; Chang, C.-S.; Li, L.-J.; Lin, T.-W. Synthesis of Large-Area MoS_2 Atomic Layers with Chemical Vapor Deposition. *Adv. Mater.* **2012**, *24*, 2320−2325.

(19) Liu, K.-K.; Zhang, W.; Lee, Y.-H.; Lin, Y.-C.; Chang, M.-T.; Su, C.-Y.; Chang, C.-S.; Li, H.; Shi, Y.; Zhang, H.; Lai, C.-S.; Li, L.-J. Growth of Large-Area and Highly Crystalline MoS_2 Thin Layers on Insulating Substrates. *Nano Lett.* **2012**, *12*, 1538−1544.

(20) Wilson, J.; Yoffe, A. The Transition Metal Dichalcogenides Discussion and Interpretation of the Observed Optical, Electrical and Structural Properties. *Adv. Phys.* **1969**, *18*, 193−335.

(21) Ataca, C.; Sahin, H.; Ciraci, S. Stable, Single-Layer MX_2 Transition-Metal Oxides and Dichalcogenides in a Honeycomb-Like Structure. *J. Phys. Chem. C* **2012**, *116*, 8983−8999.

(22) Bertolazzi, S.; Brivio, J.; Kis, A. Stretching and Breaking of Ultrathin MoS_2. *ACS Nano* **2011**, *5*, 9703−9709.

(23) Castellanos-Gomez, A.; Poot, M.; Steele, G. A.; van der Zant, H. S. J.; Agraït, N.; Rubio-Bollinger, G. Elastic Properties of Freely Suspended MoS_2 Nanosheets. *Adv. Mater.* **2012**, *24*, 772−775.

(24) Li, H.; Yin, Z.; He, Q.; Li, H.; Huang, X.; Lu, G.; Fam, D. W. H.; Tok, A. I. Y.; Zhang, Q.; Zhang, H. Fabrication of Single- and Multilayer MoS_2 Film-Based Field-Effect Transistors for Sensing NO at Room Temperature. *Small* **2012**, *8*, 63−67.

(25) Mak, K. F.; Lee, C.; Hone, J.; Shan, J.; Heinz, T. F. Atomically Thin MoS_2: A New Direct-Gap Semiconductor. *Phys. Rev. Lett.* **2010**, *105*, 136805.

(26) Yin, Z.; Li, H.; Li, H.; Jiang, L.; Shi, Y.; Sun, Y.; Lu, G.; Zhang, Q.; Chen, X.; Zhang, H. Single-Layer MoS_2 Phototransistors. *ACS Nano* **2012**, *6*, 74−80.

(27) Revolinsky, E.; Beerntsen, D. Electrical Properties of the $MoTe_2$−WTe_2 and $MoSe_2$−WSe_2 Systems. *J. Appl. Phys.* **1964**, *35*, 2086−2089.

(28) Srivastava, S.; Mandal, T.; Samantaray, B. Studies on Layer Disorder, Microstructural Parameters and Other Properties of Tungsten-Substituted Molybdenum Disulfide, $Mo_{1-x}W_xS_2$ ($0 \leq x \leq 1$). *Synth. Met.* **1997**, *90*, 135−142.

(29) Ivanovskaya, V. V.; Zobelli, A.; Gloter, A.; Brun, N.; Serin, V.; Colliex, C. *Ab Initio* Study of Bilateral Doping within the MoS_2−NbS_2 System. *Phys. Rev. B* **2008**, *78*, 134104.

(30) Schneemeyer, L. F.; Sienko, M. J. Crystal Data for Mixed-Anion Molybdenum Dichalcogenides. *Inorg. Chem.* **1980**, *19*, 789−791.

(31) Ajalkar, B.; Mane, R.; Sarwade, B.; Bhosale, P. Optical and Electrical Studies on Molybdenum Sulphoselenide $[Mo(S_{1-x}Se_x)_2]$ Thin Films Prepared by Arrested Precipitation Technique (APT). *Sol. Energy Mater. Sol. Cells* **2004**, *81*, 101−112.

(32) Agarwal, M. K.; Patel, P. D.; Talele, L. T.; Laxminarayana, D. Optical Band Gaps of Molybdenum Sulphoselenide (MoS_xSe_{2-x}, $0 \leq x \leq 2$) Single Crystals from Spectral Response. *Phys. Status Solidi A* **1985**, *90*, K107.

(33) Srivastava, S.; Palit, D. Defect Studies by X-ray Diffraction, Electrical and Optical Properties of Layer Type Tungsten Mixed Molybdenum Sulphoselenide. *Solid State Ionics* **2005**, *176*, 513−521.

(34) Popescu, V.; Zunger, A. Effective Band Structure of Random Alloys. *Phys. Rev. Lett.* **2010**, *104*, 236403.

(35) Perdew, J. P.; Burke, K.; Ernzerhof, M. Generalized Gradient Approximation Made Simple. *Phys. Rev. Lett.* **1996**, *77*, 3865.

(36) Kresse, G.; Hafner, J. *Ab Initio* Molecular Dynamics for Liquid Metals. *Phys. Rev. B* **1993**, *47*, 558−561.

(37) Kresse, G.; Furthmüller, J. Efficiency of Ab-Initio Total Energy Calculations for Metals and Semiconductors Using a Plane-Wave Basis Set. *Comput. Mater. Sci.* **1996**, *6*, 15−50.

(38) Prince, A. *Alloy Phase Equilibria*; Elsevier Publishing Co.: Amsterdam, 1966.

(39) Tenne, R.; Margulis, L.; Genut, M.; Hodes, G. Polyhedral and Cylindrical Structures of Tungsten Disulphide. *Nature* **1992**, *360*, 444−446.

(40) Komsa, H.-P.; Kotakoski, J.; Kurasch, S.; Lehtinen, O.; Kaiser, U.; Krasheninnikov, A. V. Two-Dimensional Transition Metal Dichalcogenides under Electron Irradiation: Defect Production and Doping. *Phys. Rev. Lett.* **2012**, *109*, 035503.

(41) Beal, A. R.; Hughes, H. P. Kramers−Kronig Analysis of the Reflectivity Spectra of 2H-MoS_2, 2H-$MoSe_2$ and 2H-$MoTe_2$. *J. Phys. C: Solid State Phys.* **1979**, *12*, 881.
(42) Beal, A. R.; Liang, W. Y.; Hughes, H. P. Kramers−Kronig Analysis of the Reflectivity Spectra of 3R-WS_2 and 2H-WSe_2. *J. Phys. C: Solid State Phys.* **1976**, *9*, 2449.
(43) Mak, K. F.; He, K.; Shan, J.; Heinz, T. F. Control of Valley Polarization in Monolayer MoS_2 by Optical Helicity. *Nat. Nanotechnol.* **2012**, *7*, 494−498.
(44) Zeng, H.; Dai, J.; Yao, W.; Xiao, D.; Cui, X. Valley Polarization in MoS_2 Monolayers by Optical Pumping. *Nat. Nanotechnol.* **2012**, *7*, 490−493.
(45) Xiao, D.; Liu, G.-B.; Feng, W.; Xu, X.; Yao, W. Coupled Spin and Valley Physics in Monolayers of MoS_2 and Other Group-VI Dichalcogenides. *Phys. Rev. Lett.* **2012**, *108*, 196802.